Modelling and Simulation in Materials Science and Engineering

PAPER

Development of a grain boundary pinning model that considers particle size distribution using the phase field method

To cite this article: Michael R Tonks *et al* 2015 *Modelling Simul. Mater. Sci. Eng.* **23** 045009

IOP Publishing Modelling and Simulation in Materials Science and Engineering

Modelling Simul. Mater. Sci. Eng. **23** (2015) 045009 (16pp) doi:10.1088/0965-0393/23/4/045009

Development of a grain boundary pinning model that considers particle size distribution using the phase field method

Michael R Tonks[1], Yongfeng Zhang[1], Aaron Butterfield[1,2] and Xian-Ming Bai[1]

[1] Fuel Modeling and Simulation, Idaho National Laboratory, PO Box 1625, Idaho Falls, ID 83415, US
[2] New address: Electrical and Computer Engineering, Ohio State University, 2015 Neil Ave., Columbus, OH 43210, US

E-mail: Michael.Tonks@inl.gov

Received 23 January 2015, revised 4 March 2015
Accepted for publication 25 March 2015
Published 23 April 2015

Abstract

In this work, we expand a grain boundary (GB) pinning model that considers a range of different spatial distributions of particles to also account for a distribution of particle sizes. We begin by developing a phase field model that describes GB and pore interactions and verify it by comparing to molecular dynamics simulations. We then develop an analytical pinning model that considers the impact of the particle size distribution, in terms of the mean and standard deviation of the particle radius. The analytical model is verified by comparing to simulation results of our phase field model and those of a simple Monte Carlo model. A significant finding from the model is that the *mean* value of the resistive pressure decreases with increasing *standard deviation* of the particle radius.

Keywords: zener pinning, phase field method, grain boundary migration, grain growth

(Some figures may appear in colour only in the online journal)

1. Introduction

Grain boundaries (GBs) significantly impact material performance, as they act as defect sources and sinks, inhibit dislocation motion and act as segregation sites for precipitate atoms and impurities. In addition, GBs migrate to reduce the free energy of the material system, resulting in increasing grain size over time. While the mobility of a GB is an intrinsic property,

the actual GB migration is severely influenced by impurities and defects [1, 2]. For example, particles and pores resist GB motion, slowing and even halting grain growth [3, 4].

The earliest treatment of GB pinning was by Zener [5]. Zener determined the resistive pressure for a given volume fraction of spherical, incoherent, immobile and rigid particles. Zener was able to derive a simple expression for the pinning pressure by making several simplifying assumptions; he assumed that the GBs were flat, the particles were randomly distributed, only particles within one radius influence the GBs and that all particles exert the maximum pinning force throughout the interaction. With these assumptions he derived the resistive pressure to be

$$P_r^{\max} = \frac{3}{2}\frac{\gamma_{\mathrm{GB}} f_{\mathrm{V}}^n}{r}, \tag{1}$$

where r is the particle radius, γ_{GB} is the GB energy, f_{V} is the volume fraction of particles and the exponent $n = 1$. The assumption that GBs are flat is not consistent with actual GB behavior, as GBs form a catenoid-like shape around a pinning object. In addition, as particles pin GBs, a larger fraction are located on the GBs than indicated by the assumption of flat GBs intersecting randomly distributed particles. Zener's model has been modified by later work to remove these assumptions and improve the model predictions [6–10] by employing various values of the exponent n. For example, $n = 0.93$ has been shown to account for the catenoid shape around the particles [8] and $n = 1/3$ considers particles which primarily fall on GBs [10].

An alternative approach was taken by [11]. They analyzed these various models from a stereological perspective and found that they are all significantly hindered by geometric assumptions about the particle and grain shapes and size distributions and by assumptions with regards to the spatial distributions of the particles. To address issues with regards to the spatial distribution of the particles, they investigated the resistive pressure as a function of a stereological parameter R, which quantifies the amount of GB-particle contact beyond random. Using R, they found that any spatial distribution of particles could be represented with an exponent of $n = 1$ according to

$$P_r = 2R\frac{\gamma_{\mathrm{GB}} f_{\mathrm{V}}}{\bar{\lambda}_{\mathrm{p}}}. \tag{2}$$

where $\bar{\lambda}_{\mathrm{p}}$ is the stereological particle size. Note that $\bar{\lambda}_{\mathrm{p}} = 4/3r$ for monosized spherical particles [11]. Though this approach accounts for any positioning of particles, it does not address assumptions with respect to the particle size distributions.

In this work, we seek to provide added insight into the resistance against GB migration due to particles and pores (note that for the rest of this work we say 'particle' to represent pores and particles, unless explicitly stated) with various size distributions using a combination of analytical theory and mesoscale simulation. We first summarize a phase field model of pore and GB interaction and verify it against atomistic simulation results. We also add a term to the model to apply a constant artificial force to drive GB motion. We then use a simple bicrystal system with a flat GB to study GB/particle interaction under a constant artificial driving force. We derive an equation for the resistive pressure based on the fractional coverage of the GBs by particles, i.e. the percentage of GB area currently covered by particles and compare it with the phase field results. We then modify the model to account for the particle size distribution and verify it through comparison to phase field results and results from a simple Monte Carlo model. Finally, we develop an expression for the resistive pressure for a given particle size distribution that is a function of the volume fraction, where the spatial distribution of particles is defined by the stereological parameter R as in equation (2).

2. Pore/GB interaction phase field model

In this study, we used phase field simulations to assist in the development of an expression for the resistive pressure that accounts for the particle size distribution. To ensure the accuracy of the model, we verified that the interactions between GBs and particles predicted by the phase field model were accurate by comparing to MD simulations of Helium (He) bubbles interacting with GBs in Molybdenum (Mo). Thus, we required a model that predicted these interactions, but also allowed us to prevent transport of gas atoms through the bulk or along GBs so that bubbles do not significantly change size during the simulations.

GB interaction with particles and pores have been extensively modeled with mesoscale methods. The earliest attempts used Monte Carlo Potts models [9, 12, 13] and later work applied the phase field method [14–19]. The primary benefit of the phase field model is the capability to quantitatively model the particle or pore interaction with GBs [14, 20–23].

We employed a simple phase field model of pore and GB interaction based on that presented in [22]. However, we added the directional model of bulk, surface and GB diffusion from [24]. In the model, grains are represented by order parameters η_i equal to one within a corresponding grain and equal to zero in the other grains and within pores, assuming isotropic GB properties. The pores are represented with a conserved vacancy concentration c that is equal to one within a pore and some small concentration in the bulk. The variables evolve to minimize the total free energy in the system, representing microstructure evolution. The free energy of the system is defined in terms of the model variables as [22]

$$F = \int_{\mathrm{V}} \left(\mu f(c, \eta_i) + \frac{\kappa_{\mathrm{c}}}{2} |\nabla c|^2 + \sum_i \frac{\kappa_i}{2} |\nabla \eta_i|^2 \right) \mathrm{d}V, \tag{3}$$

where κ_{c} is the interfacial parameter for c, κ_i is the interfacial parameter for the ith order parameter and μ is the bulk energy parameter. The bulk energy term is defined as

$$f(c, \eta_i) = \sum_i \left(\frac{\eta_i^4}{4} - \frac{\eta_i^2}{2} \right) + \left(\frac{c^4}{4} - \frac{c^2}{2} \right) + a_{\mathrm{GB}} \sum_i \sum_{j>i} \eta_i^2 \eta_j^2 + a_{\mathrm{s}} \sum_i c^2 \eta_i^2, \tag{4}$$

where a_{GB} is set to 1.5 to ensure a symmetric diffuse interface [25] and $a_{\mathrm{s}} = a_{\mathrm{GB}}\, \gamma_{\mathrm{s}}/\gamma_{\mathrm{GB}}$ with surface energy γ_{s} and GB energy γ_{GB}.

The evolution of the concentration c is defined by a Cahn–Hilliard equation according to

$$\frac{\partial c}{\partial t} = \nabla \cdot \mathbf{M} \nabla \frac{\delta F}{\delta c(\mathbf{r}, t)}, \tag{5}$$

where $\mathbf{r}$ is the spatial position, t is the time and $\mathbf{M}$ is the concentration mobility rank two tensor that accounts for directional diffusion along surfaces and GBs. The evolution of the order parameters η_i is defined by an Allen–Cahn equation, as

$$\frac{\partial \eta_i}{\partial t} = -L \frac{\delta F}{\delta \eta_i(\mathbf{r}, t)}, \tag{6}$$

where L is the scalar order parameter mobility and for this model is assumed to be equal for all GBs.

The model has a number of parameters that must be determined as functions of measurable quantities in order to make a material specific model. These quantities are the GB energy γ_{GB}, surface energy γ_{s}, effective vacancy or gas diffusivity D_{eff} and the GB mobility M_{GB}. For the order parameter values, we use the model presented in [25], which gives the relationships

$$\kappa_i = \frac{3}{4}\gamma_{\mathrm{GB}} l_{\mathrm{GB}} \tag{7}$$

$$L = \frac{4}{3}\frac{M_{\mathrm{GB}}}{l_{\mathrm{GB}}} \tag{8}$$

$$\mu = 6\frac{\gamma_{\mathrm{GB}}}{l_{\mathrm{GB}}}. \tag{9}$$

where l_{GB} is the interfacial width that defines the width of the diffuse interfaces in the phase field model and $M_{\mathrm{GB}} = M_0 \mathrm{e}^{-\frac{Q}{k_{\mathrm{b}}T}}$ is the GB mobility with the mobility prefactor M_0 and the activation energy Q. The magnitude of the concentration mobility tensor $\mathbf{M}$ can be determined by the fact that the concentration evolution in the bulk should follow Fick's law of diffusion for $c \ll 1$, such that

$$\mathbf{M} = \mathbf{D}/\frac{\partial^2 F}{\partial c^2} = \mathbf{D}/(\mu(2a_{\mathrm{s}} - 1)). \tag{10}$$

The concentration c impacts the free energy in the same manner as η_i, therefore

$$\kappa_{\mathrm{c}} = \frac{3}{4}\gamma_{\mathrm{s}} l_{\mathrm{GB}}. \tag{11}$$

The gas diffusivity matrix defines the total diffusivity due to bulk, surface and GB diffusion following the model from [24]. The diffusivity matrix is equal to

$$\mathbf{D} = D_{\mathrm{eff}}(\hat{\mathbf{D}}_b + \hat{\mathbf{D}}_{\mathrm{s}} + \hat{\mathbf{D}}_{\mathrm{GB}}), \tag{12}$$

where the effective diffusivity

$$D_{\mathrm{eff}} = D_0 \mathrm{e}^{-\frac{E_{\mathrm{m}}}{k_{\mathrm{b}}T}} \tag{13}$$

with the diffusivity prefactor D_0, migration energy E_{m}, Boltzmann constant k_{b} and temperature T. The individual normalized diffusivity tensors for bulk diffusivity ($\hat{\mathbf{D}}_b$), surface diffusivity ($\hat{\mathbf{D}}_{\mathrm{s}}$) and GB diffusivity ($\hat{\mathbf{D}}_{\mathrm{GB}}$) are determined as

$$\hat{\mathbf{D}}_b = w_b \mathbf{I} \tag{14}$$

$$\hat{\mathbf{D}}_{\mathrm{s}} = w_{\mathrm{s}} c^2 (1 - c^2) \mathbf{T}_{\mathrm{s}} \tag{15}$$

$$\hat{\mathbf{D}}_{\mathrm{GB}} = w_{\mathrm{GB}} \sum_{i=1} \sum_{j \neq i} \eta_i \eta_j \mathbf{T}_{\mathrm{GB}}, \tag{16}$$

where w_b, w_{s} and w_{GB} are weighting parameters and T_{s} and T_{GB} are surface and GB projection tensors, respectively. The surface projection tensor is a function of the concentration according to

$$T_{\mathrm{s}} = \mathbf{I} - \frac{\nabla c}{|\nabla c|} \otimes \frac{\nabla c}{|\nabla c|}. \tag{17}$$

The GB projection tensor is a function of the order parameters as

$$T_{\mathrm{GB}} = \mathbf{I} - \frac{\nabla\eta_i - \nabla\eta_j}{|\nabla\eta_i - \nabla\eta_j|} \otimes \frac{\nabla\eta_i - \nabla\eta_j}{|\nabla\eta_i - \nabla\eta_j|}. \tag{18}$$

The weights w_b, w_s and w_{GB} define the relative importance of the bulk diffusion, surface diffusion and GB diffusion, respectively. In order to restrict transport of gas through the bulk and prevent gas bubble growth/shrinkage, we used the parameter values $w_b = w_{\mathrm{GB}} = 1 \times 10^{-4}$ and $w_\mathrm{s} = 1.0$.

To simplify our investigation of the resistive pressure, we apply a constant artificial driving force to the GBs. The artificial driving force is added to the model by adding an additional term to equation (6) according to

$$\frac{\partial\eta_i}{\partial t} = -L\left(\frac{\delta F}{\delta\eta_i} + A\mathbf{f}_\mathrm{d} \cdot \nabla\eta_i\right). \tag{19}$$

To derive an expression for A, we use a similar approach to that taken in [26]. The velocity of a GB moving due to this driving force is $v = M_{\mathrm{GB}} f_\mathrm{d}$. The velocity of a flat GB (i.e. $\partial F/\partial\eta_i = 0$) that is perpendicular to the x-axis in the phase field model using equation (19) is

$$v = \frac{\partial\eta_i}{\partial t} \Big/ \frac{\partial\eta_i}{\partial x} = -LAf_\mathrm{d}. \tag{20}$$

If we equate these two expressions for v, substitute in equation (8) and solve for A, we obtain

$$A = -\frac{3}{4} l_{\mathrm{GB}}. \tag{21}$$

The magnitude of the driving force used in this work is $f_\mathrm{d} = 21.1$ MPa in the x-direction. This driving force is comparable in magnitude to the curvature driving force for a grain size of 0.2 μm.

The phase field equations are solved using the finite element method using the MARMOT mesoscale modeling code as outlined in [27]. The concentration is solved by splitting the fourth order Cahn–Hilliard equation into two second-order equations in the manner summarized in [28]. All of the equations are solved simultaneously using implicit time integration. We employed mesh adaptivity to reduce the computational expense.

To model GB and pore interaction in the Mo–He system, we required values for the GB mobility and energy in Mo. We also needed the diffusivity prefactor D_0 and the migration energy E_m to calculate the diffusivity, as well as the Mo surface energy γ_s. We obtained these values (shown in table 1) from molecular dynamics (MD) simulations. In the MD simulations we used the interatomic potential developed in Ackland *et al* [29] for pure Mo and that in Zhang *et al* [30] for He–Mo. The GB energy and mobility were obtained using the circular-embedded grain model [31] with $\langle 100 \rangle$ 45° tilt GBs. For the surface energy, the result is calculated using a spherical void with a 12 nm diameter.

In order to verify that the phase field model accurately captures the interaction between pores and GBs, we compared the phase field results to MD simulation results representing identical Mo systems containing He bubbles. The reduction in volume of a circular grain with an initial radius of 20 nm was predicted by both simulation approaches, with ten bubbles randomly distributed along the GB. The 3D domain was 64.4 nm × 64.4 nm × 1.93 nm with periodic boundary conditions and the center axis of the circular grain was parallel with the z-axis. The ten He bubbles had a radius of 0.3 nm (ten He atoms were used to represent the

Table 1. Properties of the Mo–He system used in the phase field simulations calculated using MD.

Property	Value
D_0	3.325×10^{-10} m^2 s^{-1}
E_m	0.999 eV
γ_GB	1.920 J m^{-2}
σ_s	2.160 J m^{-2}
M_0	3.986×10^{-6} m^4 Js^{-1}
Q	1.031 eV

bubbles in the MD simulations). The simulations were carried out at a temperature of 2700 K. Three simulations were run with different random initial positions of the ten He bubbles using both approaches. The phase field simulations employed a GB width of $l_\mathrm{GB} = 0.2$ nm. Examples of the phase field and MD domains are shown in figure 1(*a*).

Both approaches predicted an initially slow reduction in the grain volume (see figure 1(*b*)), while all ten bubbles are in contact with the GB. However, the rate increases as the GB releases from more and more of the ten bubbles until the final rate of reduction is defined by the intrinsic GB mobility, as no bubbles are in contact with the GB. The comparison between these two distinct methods is reasonably good, though the phase field simulations seem to predict somewhat slower decrease in the grain size at the early stages of the volume reduction. Thus, we confidently employed phase field models to inform the development of an analytical model of the resistive pressure that accounts for a particle size distribution.

3. The analytical resistive pressure model

In Zener's original model, he considered the resistive force of spherical, incoherent, immobile and rigid particles on migrating GBs. This resistive force is equal to

$$F_r = 2\pi r \gamma_\mathrm{GB} \cos\beta \sin\beta, \tag{22}$$

where r is the particle radius and β the angle illustrated in figure 2. He determined that the maximum force occurs at $\beta = 45°$, such that

$$F_r^\mathrm{max} = \pi r \gamma_\mathrm{GB}. \tag{23}$$

Similar expressions have been derived using the argument that the particle takes the place of some GB area, reducing the GB energy [7]. By making the simplifying assumptions mentioned previously, Zener determined that the resistive pressure is equal to equation (1). The GB velocity is a function of the GB mobility M, the driving pressure P and the resistive pressure P_r according to

$$v = M(P - P_r), \tag{24}$$

where $P_r \leqslant P$.

Zener based his resistive pressure on the volume fraction of particles f_V, as this is an observable and measurable quantity to allow for validation of the model and facilitate its applicability in real systems. However, to quantify the resistive pressure as a function of the volume fraction, he had to assume random positioning of particles with respect to GBs.

Here, we derive an expression that makes no assumptions about the positioning of the particles by basing it directly on the GB fractional coverage f_c, or the percentage of GB area

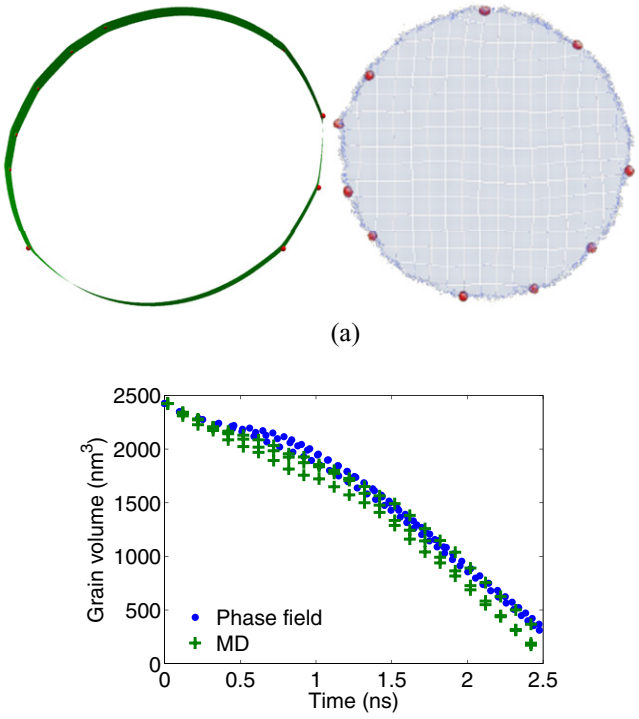

Figure 1. Verification of the phase field model by comparing to MD results. A shrinking Mo circular grain with ten He bubbles distributed along the grain boundary is modeled by both approaches, where examples of the phase field (left) and MD (right) simulation domains are shown in (*a*). The volume of the shrinking grain versus time predicted by both methods is shown in (*b*). Note that points from three different simulations for each approach with different initial bubbles positions are shown in the plot. The phase field results show reasonably good agreement with the MD results.

currently covered by particle area. We begin with the resistive force, from equation (22) and multiply by the the number of particles per unit area in contact with the GB to get the resistive pressure

$$P_r = 2\pi r \gamma_{\mathrm{GB}} \cos\beta \sin\beta \frac{N_{\mathrm{p}}^{\mathrm{GB}}}{A_{\mathrm{GB}}}, \tag{25}$$

where $N_{\mathrm{p}}^{\mathrm{GB}}$ is the total number of particles in contact with the GB, A_{GB} is the total GB area and we assume that all particles interact with the GB with the same angle β. If we substitute in the expression for the fractional coverage $f_{\mathrm{c}} = N_{\mathrm{p}}^{\mathrm{GB}} A_b / A_{\mathrm{GB}}$, we obtain

$$P_r = 2\pi r \gamma_{\mathrm{GB}} \cos\beta \sin\beta \frac{f_{\mathrm{c}}}{A_b} \tag{26}$$

$$= \frac{2\gamma_{\mathrm{GB}} f_{\mathrm{c}} \cos\beta \sin\beta}{r} \tag{27}$$

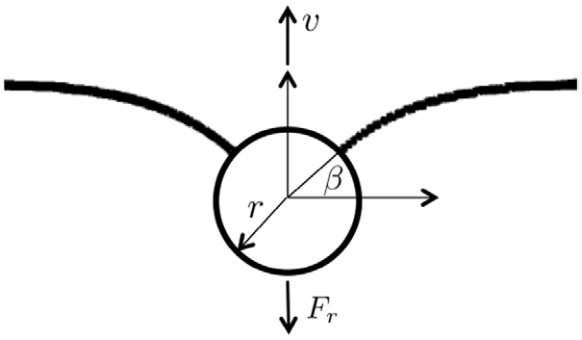

Figure 2. Illustration of the interaction between a particle and a GB that meet at an angle β, where r is the particle radius, v is the GB velocity and F_r is the resistive force caused by the particle.

where $A_b = \pi r^2$ is the cross section of a single particle on the GB. The max resistive pressure would occur at $\beta = 45°$ with a value of

$$P_r^{\max} = \frac{\gamma_{\mathrm{GB}} f_{\mathrm{c}}}{r}. \tag{28}$$

The relationship between the fractional coverage and the volume fraction depends on the spatial distribution of the particles and is discussed in section 5 of this work.

As the GB passes the pinning particles, it does not stay flat but rather takes on a catenoid shape, as shown in figure 2. To account for the catenoid shape, Zener's model was modified with the exponent $n = 0.93$ [8], thus increasing the resistive pressure. To account for the catenoid shape in our model, we include a weighting term W to give

$$P_r = 2W \frac{\gamma_{\mathrm{GB}} f_{\mathrm{c}} \cos\beta \sin\beta}{r} \tag{29}$$

$$P_r^{\max} = W \frac{\gamma_{\mathrm{GB}} f_{\mathrm{c}}}{r}.$$

The value for W was determined by comparing to phase field simulations of GB migration with pinned boundaries.

We modeled a Mo bicrystal with dimensions of 0.2 μm $\times$ 0.4 μm $\times$ 0.4 μm, with a flat GB driven by the artificial driving force at $T = 800$ K using the values from table 1. Because the domain size was larger than in the previous simulation, we employed a larger GB width of $l_{\mathrm{GB}} = 3.1$ nm to allow for a larger minimum mesh size to reduce the computational expense. Various numbers of He bubbles were lined up in the path of the migrating GB on a plane parallel to the GB plane, as shown in figure 3(*a*). In each simulation, all bubbles had the same radius and simulations were run using radii of 7.0, 9.0 and 11.0 nm. The 3D simulations were run on 480 processors for approximately 48 h.

A plot of the grain volume versus time for various numbers of 11 nm radius bubbles is shown in figure 3(*b*). Note that the change in volume of the grain is linear until the GB comes in contact with the bubbles. At this time, the rate increases as the GB is pulled towards the bubbles. This is consistent with the resistive force equation (equation (22)) for values of β less then zero. As the GB moves past the bubbles, the velocity of the GB decreases until the GB reaches an angle of $\beta = 45°$, where the resistive force is maximum. The GB maintains a fairly

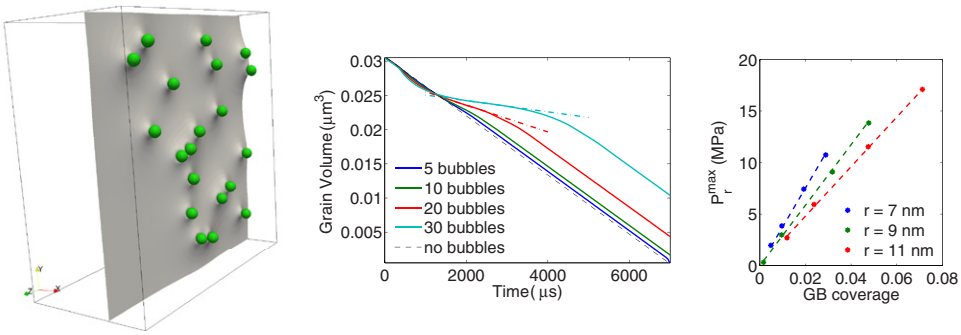

(a) (b) (c)

Figure 3. Comparison between the analytical model (equation (29)) and phase field simulation results modeling a flat GB driven by an artificial driving force and interacting with aligned bubbles with a single constant radius. An example of a phase field simulation with twenty $r = 9$ nm radius bubbles is shown in (*a*), the grain volume of the shrinking grain versus time predicted by the phase field simulations for various numbers of aligned $r = 11$ nm bubbles is shown in (*b*) (where the linear fits used to calculate the maximum resistive pressure are shown as dash–dotted lines for the 20 and 30 bubble simulations) and the comparison of the maximum resistive pressure predicted by the analytical model to that obtained from the phase field simulations is shown in (*c*). The fit value of $W = 1.1$ seems to be independent of bubble radius and number of bubbles for this system.

constant velocity for some time at this point of maximum resistive force, until bubbles begin to be released from the GB. Eventually, the GB releases from all bubbles and its rate returns to its value before it came in contact with the bubbles. Though all the curves follow this same trend, the magnitude of the changes in velocity increase with increasing numbers of bubbles.

To simplify the comparison between our phase field results and the analytical equation defining the resistive pressure as a function of the fractional coverage, we focus on the time at which the contact angle β is near 45°, when the resistive force is a maximum. To determine the GB velocity, we fit a line to the phase field data (shown for the 20 and 30 bubble simulations in figure 3(*b*)) during this period and use the slope to calculate the velocity. From this velocity, we calculate $P_r^{\max}$ from equation (24) and the value of the artificial driving force.

We determined the value for W by fitting equation (29) to the values for $P_r^{\max}$ calculated from the simulation results with $r = 7$ nm, giving $W = 1.1$. Using this value, we compared the model predictions to the phase field results for $r = 9$ nm and $r = 11$ nm, as shown in figure 3(*c*). The phase field results clearly show a linear relationship between $P_r^{\max}$ and f_c and an inverse relationship with the bubble radius. In addition, the predicted values compare closely with the phase field results, which seems to indicate that the value for W is independent of the value of f_c and r for this system.

As a final test of the analytical model and the W value, we compared the analytical model predictions from equation (29) to the circular grain results from figure 1. Since the bubbles do not detach from the GB simultaneously, the number of bubbles in contact with the GB was recorded from the simulation and used to calculate the value of f_c over time. As the GB migrates through the ten He bubbles, the β contact angle is different for each bubble, varying from approximately $-45°$ to 45°. However, we found that an average contact angle of 18° provided the best comparison with the phase field results, probably because the GB spends the most time near $\beta = 45°$, pushing the average above 0°. The model predictions compare well

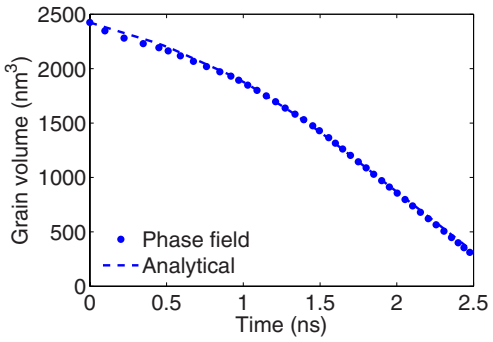

Figure 4. Comparison between the phase field simulation results for a circular grain with ten bubble and the analytical model (equation (29)), showing excellent agreement. Note that f_c for the model is estimated from the number of bubbles in contact with the GB and an average contact angle value $\beta = 18°$ (as the transient contact angle is different for each bubble) was found to produce the best comparison with the phase field results.

with the simulation results, as shown in figure 4, providing some evidence that W is independent of driving force.

4. Resistive pressure model with a particle size distribution

Both Zener's pinning model from equation (1) (for randomly distributed particles) and our new model from equation (29) (for any spatial distribution) define the resistive pressure for particles with the same radius r. However, in reality the particles will have a distribution of sizes and the variation in the particle radius could impact the resistive pressure. In this section we modify equation (29) to account for the particle size distribution.

For a set of particles with radii that vary according to a given probability density function $f(\tilde{r})$, the resistive pressure becomes a stochastic function, as does the GB fractional coverage. To determine the expected, or average, value of the stochastic resistive pressure $E(\tilde{P}_r^{\max})$ we must account for the stochastic nature of the fractional coverage. For a given fractional coverage f_c and known particle radius distribution with mean $\bar{r}$ and standard deviation σ_r, the total maximum resistive pressure due to particles with varying radii $\tilde{r}$ can be expressed by modifying equation (29) to obtain

$$\tilde{P}_r^{\max} = W\gamma_{GB} \sum_{i=1}^{N_p^{GB}} \frac{f_c(\tilde{r}_i)}{\tilde{r}_i}, \tag{30}$$

where N_p^{GB} is the number of particles on the GB and the fractional coverage for a single particle $f_c(\tilde{r}_i) = \pi\tilde{r}_i^2/A_{GB}$ with the grain boundary area A_{GB}. The expected value of the resistive pressure is

$$E\left(\tilde{P}_r^{\max}\right) = \frac{W\gamma_{GB}\pi}{A_{GB}} E\left(\sum_{i=1}^{N_p^{GB}} \tilde{r}_i\right) = \frac{W\gamma_{GB}\pi}{A_{GB}} N_p^{GB}\bar{r}. \tag{31}$$

The fractional coverage can be calculated from

$$\tilde{f}_c = \sum_{i=1}^{N_p^{GB}} \frac{\pi \tilde{r}_i^2}{A_{GB}}. \tag{32}$$

As f_c is known, it is equal to the expected value according to

$$f_c = E(\tilde{f}_c) = \frac{\pi}{A_{GB}} E\left(\sum_{i=1}^{N_p^{GB}} \tilde{r}_i^2 \right) = \frac{\pi}{A_{GB}} N_p^{GB} (\bar{r}^2 + \sigma_i^2), \tag{33}$$

where $E(\tilde{r}_i^2) = \bar{r}^2 + \sigma_i^2$, from the definition of the standard deviation. Solving this expression for N_p^{GB} and substituting into equation (31) gives

$$E(\tilde{P}_r^{max}) = \frac{\bar{r}^2}{\bar{r}^2 + \sigma_r^2} W \frac{\gamma_{GB} f_c}{\bar{r}}$$

$$= \frac{1}{1 + \left(\frac{\sigma_r}{\bar{r}}\right)^2} W \frac{\gamma_{GB} f_c}{\bar{r}}. \tag{34}$$

This expression is equivalent to equation (29) when the standard deviation is zero and it indicates that the value of the resistive pressure decreases as the square of the ratio of the standard deviation to the mean of the particle radius increases. Thus, equation (29) defines the upper bound of the pinning pressure and is a good approximation for small ratios of σ_r to $\bar{r}$.

As with the deterministic model, we verified this model by comparing to phase field simulation results. These simulations were similar to those from the previous section, but the bubble radii were randomly sampled from a normal distribution with a given mean and standard deviation. We conducted a series of simulations with a mean bubble radius $\bar{r} = 11$ nm and standard deviation $\sigma_r = 2$ nm (see figure 5(*a*)), which predicted resistive pressures in good agreement with the analytical model (figure 5(*b*)). However, accurately verifying the statistics from the phase field simulation results would require hundreds of simulations, which would be computationally prohibitive. Therefore, we developed a Monte Carlo model for further verification. In the model, random radii $\tilde{r}_i$ are generated from a normal distribution for N_p^{GB} bubbles in contact with the GB. The stochastic resistive pressure is generated according to equation (30) (with $W = 1.1$) and the total stochastic fractional coverage is calculated from equation (32). For each number of bubbles for a given bubble radius mean and standard deviation, the stochastic model was applied for 10 000 different sets of random bubble radii.

The expected values of the resistive pressure $E(\tilde{P}_r^{max})$ predicted by equation (34) compared well with the values predicted by the Monte Carlo model and by the phase field simulations with random bubble radii, as shown in figure 5(*b*). A significant finding from this work is that for a given fractional coverage, the mean value of the resistive pressure is a function of the standard deviation, as shown in equation (34) and demonstrated in figure 5(*c*). The results also demonstrate that the impact of a given particle radius standard deviation decreases as the mean radius increases (see figure 5(*c*)).

5. Model with a particle size distribution in terms of the volume fraction

Equation (34) defines the resistive force due to spherical particles with radii that vary according to a normal distribution as a function of the fractional coverage f_c. However, f_c is difficult

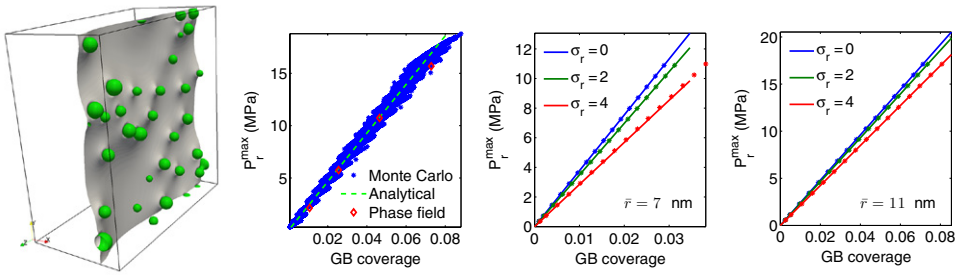

Figure 5. Verification of our resistive pressure model that is a function of the GB fractional coverage and considers particle size distributions (equation (34)). An example of a phase field simulation with bubble radii following a normal distribution with a mean radius of $\bar{r} = 11$ nm and standard deviation of $\sigma_r = 2$ nm is shown in (*a*), a comparison of the analytical model, Monte Carlo results and the phase field simulations for $\bar{r} = 11$ nm and $\sigma_r = 2$ nm is shown in (*b*) and the analytical model shows excellent agreement with the phase field simulations and the Monte Carlo model. The variation of the resistive pressure with standard deviation for two mean radii is shown in (*c*), where the line shows the analytical model and the symbols show the mean values from the Monte Carlo simulations.

to measure and changes with time. In general, the volume fraction f_V is a much more valuable means of quantifying the particle density. To modify equation (34) to be a function of f_V requires a relationship between the GB fractional coverage f_c and the volume fraction f_V for various spatial distributions of particles. The stereological parameter R from [4] can represent any spatial distribution, therefore we developed a relationship between f_c and f_V using R for particles with a given size distribution.

The stereological parameter R quantifies the amount of GB-particle contact beyond random, i.e.

$$R = \frac{f_V^{GB}}{f_V}, \tag{35}$$

where f_V^{GB} is the volume fraction of particles in a volume for which average particles could be in contact with the GB, i.e. $V_{GB} = 2A_{GB}\bar{r}$, where A_{GB} is the GB area. When the particles are randomly distributed, $f_V^{GB} = f_V$ and $R = 1$. From this definition of R, we can derive an expression for the GB coverage f_c that is a function of the known volume fraction f_V,

$$f_c = \frac{3Rf_V}{2}\frac{\bar{r}(\bar{r}^2 + \sigma_r^2)}{\bar{r}^3 + 3\bar{r}\sigma_r^2}, \tag{36}$$

where the derivation is shown in the appendix. If we substitute this expression into equation (34), we obtain

$$E(\tilde{P}_r^{max}) = \frac{\bar{r}^3}{\bar{r}^3 + 3\bar{r}\sigma_r^2}\frac{3}{2}WR\frac{\gamma_{GB}f_V}{\bar{r}}$$

$$= \frac{1}{1 + 3\left(\frac{\sigma_r}{\bar{r}}\right)^2}\frac{3}{2}WR\frac{\gamma_{GB}f_V}{\bar{r}}. \tag{37}$$

The expression is again a function of the square of the ratio of the standard deviation to the mean of the particle radius, as in equation (34). When the standard deviation of the particle radius is equal to zero, this expression becomes

$$P_r^{\max} = \frac{3}{2} WR \frac{\gamma_{\mathrm{GB}} f_{\mathrm{V}}}{r}, \tag{38}$$

which is equivalent to equation (2) for $W = 1$, from [11]. For particles with the standard deviation of the particle radius equal to zero and a random spatial distribution ($R = 1$), the expression becomes identical to Zener's equation (1) for $W = 1$.

We verified this model by again comparing to Monte Carlo simulation results. We randomly selected the particle radii as done in the model from the previous section, however we now also randomly selected a uniformly distributed center location for each particle. For a given GB location, only particles for which their center location is within their radius of the GB location contribute to the maximum resistive pressure calculated with equation (34) (with $W = 1.1$), though all particles are included in the calculation of the volume fraction. A number of GB locations were employed and $\tilde{P}_r^{\max}$ was calculated for 10 000 sets of randomly selected particle radii and locations. The analytical model compared well with the expected value of the Monte Carlo simulation, as shown in figure 6.

Equation (37) predicts the resistive pressure for particles with a spatial distribution defined by the stereological parameter R and with a given size distribution with a mean particle radius of $\bar{r}$ and a radius standard deviation of σ_r. As the square of the ratio of the standard deviation of the radius to its mean increases, the resistive pressure decreases, as shown in figure 6. Thus, a given standard deviation has a smaller impact on a system with a larger mean particle radius. In addition, equation (2) [11] provides an upper bound for the resistive pressure. From this result, it can be concluded that previous work that has not considered the impact of the particle size distribution has tended to over predict the resistive pressure, though not significantly if the ratio of the standard deviation to the mean particle radius was small. While we have verified equation (37) in this work, comparisons with experimental grain growth data with known particle size distributions are required to validate the model.

It can facilitate experimental validation to capture the particle pinning effect through an effective mobility M_{eff}, rather than the resistive pressure as done in equation (24). Thus, we end this work by defining an effective mobility for particles with a spatial distribution defined by R and with a given particle size distribution. To accomplish this, equation (24) is equated to the GB velocity of an effective system without a resistive pressure and we solve for M_{eff}, i.e.

$$\begin{aligned} M_{\mathrm{eff}} P &= M(P - P_r) \\ M_{\mathrm{eff}} &= M\left(1 - \frac{P_r}{P}\right). \end{aligned} \tag{39}$$

If we assume that the driving force is due to curvature, such that $P = 2\gamma_{\mathrm{GB}}/d$, where d is the grain size, we can obtain a final expression for the effective mobility by substituting equation (37) into equation (39) to obtain

$$M_{\mathrm{eff}} = M\left(1 - \frac{1}{1 + 3\left(\frac{\sigma_r}{\bar{r}}\right)^2} \frac{3}{4} \frac{WRf_{\mathrm{V}} d}{\bar{r}}\right) \tag{40}$$

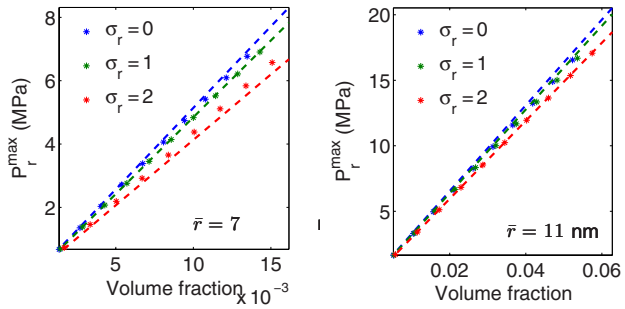

Figure 6. Verification of the analytical model that is a function of the volume fraction and accounts for the impact of a particle size distribution (equation (37)) using Monte Carlo simulations for particles with random spatial distribution, where the dashed lines show the analytical model and the symbols show the the mean values from the Monte Carlo simulations. The analytical model compares well with the Monte Carlo results for an average radii of $\bar{r} = 7$ nm (left) and $\bar{r} = 11$ nm (right).

6. Conclusions

Particles and pores resist GB motion, applying an opposing pressure. Here we add to the significant work that has been done in the past looking at the impact of different spatial distributions of particles with respect to the GBs by developing an expression that accounts for a particle size distribution. We first developed a phase field model that accounts for pore and GB interaction and verified it by comparing to MD simulation results. We then developed an analytical model for the resistive pressure that is a function of the GB fractional coverage rather than the particle volume fraction. We used results from phase simulations of a flat GB driven with an artificial driving force interacting with pores to determine a parameter value to account for the GB catenoid shape that forms around particles. We then modified the model to account for a particle size distribution and verified it by comparing to phase field and Monte Carlo simulation results. Finally, we developed an expression for the resistive pressure for a given particle size distribution that is a function of the volume fraction, where the spatial distribution of particles is defined by the stereological parameter R as in [11]. A significant finding from the model is that the *mean* resistive pressure decreases as the *standard deviation* of the bubble radius increases. Note that the model needs to be validated by comparing to experimental grain growth data with known particle size distributions.

Acknowledgments

This work was funded by the Department of Energy Nuclear Energy Advanced Modeling and Simulation program. This manuscript has been authored by Battelle Energy Alliance, LLC under Contract No. DE-AC07-05ID14517 with the US Department of Energy. The United States Government retains and the publisher, by accepting the article for publication, acknowledges that the United States Government retains a nonexclusive, paid-up, irrevocable, worldwide license to publish or reproduce the published form of this manuscript, or allow others to do so, for United States Government purposes.

Appendix A.

Here, we derive an expression for the fractional coverage f_c in terms of the stereological parameter R and the volume fraction f_V for particles with a distribution of particles sizes. For this derivation, we assume that all particles in the material have a radius that follows the same distribution with mean $\bar{r}$ and standard deviation σ_r. We define R as

$$R = \frac{f_V^{GB}}{f_V}, \tag{A.1}$$

where f_V^{GB} is the volume fraction of particles in a volume for which average particles could be in contact with the GB, i.e. $V_{GB} = 2A_{GB}\bar{r}$. This volume fraction can be calculated according to

$$f_V^{GB} = \frac{N_p^{GB}\bar{V}_b}{V_{GB}}, \tag{A.2}$$

where N_p^{GB} is the number of particles in contact with the GB and $\bar{V}_b$ is the mean value of the bubble volume. The total volume fraction can be expressed as

$$f_V = \frac{N_p\bar{V}_b}{V_m}, \tag{A.3}$$

where N_p is the total number of particles and V_m is the total volume of the material. Substituting equations (A.2) and (A.3) into equation (A.1) gives

$$R = \frac{N_p^{GB}}{N_p}\frac{V_m}{2A_{GB}\bar{r}}. \tag{A.4}$$

To make the above equation be a function of f_c and f_V requires expressions for N_p^{GB} and N_p. Solving equation (33) for N_p^{GB} gives

$$N_p^{GB} = \frac{f_c A_{GB}}{\pi(\bar{r}^2 + \sigma_r^2)}. \tag{A.5}$$

To obtain an expression for N_p, we calculate the stochastic volume fraction from

$$\tilde{f}_V = \frac{4\pi}{3V_m}\sum_{i=1}^{N_p}\tilde{r}_i^3. \tag{A.6}$$

The volume fraction f_V is known and is equal to the expected value of the stochastic volume fraction, i.e.

$$f_V = E(\tilde{f}_V) = \frac{4\pi}{3V_m}E\left(\sum_{i=1}^{N_p}\tilde{r}_i^3\right) = \frac{4\pi}{3V_m}N_p E(\tilde{r}^3). \tag{A.7}$$

To determine the expected value of $\tilde{r}^3$, we assume $\tilde{r}$ is a normally distributed variable with $\tilde{r} = \bar{r} + \sigma_r\tilde{z}$, where σ_r is the standard deviation of $\tilde{r}$ and $\tilde{z}$ is a standard normal variable ($\bar{z} = 0$ and $\sigma_z = 1$). Thus the expected value of r^3 can be obtained from

$$\begin{aligned} E(r^3) &= E(\bar{r}^3 + 3\bar{r}^2\sigma_r z + 3\sigma_r^2 z^2\bar{r} + \sigma_r^3 z^3) \\ &= \bar{r}^3 + 3\sigma_r^2\bar{r}, \end{aligned} \tag{A.8}$$

where the expected value of z^2 is one and of z^3 is zero. Substituting this expression into equation (A.7) and solving for N_p gives

$$N_p = \frac{3}{4}\frac{f_V V_m}{\pi(\bar{r}^3 + 3\bar{r}\sigma_r^2)} \tag{A.9}$$

We then substitute equations (A.5) and (A.9) into equation (A.4) to give

$$R = \frac{2}{3}\frac{f_c(\bar{r}^3 + 3\bar{r}\sigma_r^2)}{f_V \bar{r}(\bar{r}^2 + \sigma_r^2)}. \tag{A.10}$$

By solving this equation for f_c we obtain

$$f_c = \frac{3Rf_V}{2}\frac{\bar{r}(\bar{r}^2 + \sigma_r^2)}{\bar{r}^3 + 3\bar{r}\sigma_r^2}. \tag{A.11}$$

References

[1] Cahn J W 1962 *Acta Metall.* **10** 789–98
[2] Michels A, Krill C, Ehrhardt H, Birringer R and Wu D 1999 *Acta Mater.* **47** 2143–52
[3] Doherty R, Srolovitz D, Rollett A and Anderson M 1987 *Scr. Metall.* **21** 675–9
[4] Patterson B R and Liu Y 1990 *J. Am. Ceram. Soc.* **73** 3703–5
[5] Zener C quoted by Smith C 1948 *Trans. Met. Soc. AIME* **175** 15–51
[6] Gladman T 1966 *Proc. R. Soc. Lond.* A **294** 298–309
[7] Ashby M, Harper J and Lewis J 1969 *Trans. Met. Soc. AIME* **245** 413–20
[8] Hellman P and Hillert M 1975 *Scand. J. Met.* **4** 211
[9] Srolovitz D, Anderson M, Sahni P and Grest G 1984 *Acta Metall.* **32** 793–802
[10] Hillert M 1988 *Acta Metall.* **36** 3177–81
[11] Liu Y and Patterson B 1996 *Acta Mater.* **44** 4327–35
[12] Anderson M, Grest G, Doherty R, Li K and Srolovitz D 1989 *Scr. Metall.* **23** 753–8
[13] Miodownik M, Holm E A and Hassold G N 2000 *Scr. Mater.* **42** 1173–7
[14] Fan D, Chen L-Q and Chen S-P P 1998 *J. Am. Ceram. Soc.* **81** 526–32
[15] Moelans N, Blanpain B and Wollants P 2005 *Acta Mater.* **53** 1771–81
[16] Moelans N, Blanpain B and Wollants P 2006 *Acta Mater.* **54** 1175–84
[17] Moelans N, Blanpain B and Wollants P 2007 *Acta Mater.* **55** 2173–82
[18] Millett P, Wolf D, Desai T, Rokkam S and El-Azab A 2008 *J. Appl. Phys.* **104** 033512
[19] Wang N, Wen Y and Chen L-Q 2014 *Phil. Mag. Lett.* **94** 794–802
[20] Millett P C, El-Azab A, Rokkam S, Tonks M and Wolf D 2011 *Comput. Mater. Sci.* **50** 949–59
[21] Millett P C, El-Azab A and Wolf D 2011 *Comput. Mater. Sci.* **50** 960–70
[22] Millett P C and Tonks M 2011 *J. Nucl. Mater.* **412** 281–6
[23] Chang K and Chen L-Q 2012 *Modelling Simul. Mater. Sci. Eng.* **20** 055004
[24] Ahmed K, Yablinsky C, Schulte A, Allen T and El-Azab A 2013 *Modelling Simul. Mater. Sci. Eng.* **21** 065005
[25] Moelans N, Blanpain B and Wollants P 2008 *Phys. Rev.* B **78** 024113
[26] Tonks M R, Zhang Y, Bai X and Millett P C 2014 *Mater. Res. Lett.* **2** 23–8
[27] Tonks M, Gaston D, Millett P, Andrs D and Talbot P 2012 *Comput. Mater. Sci.* **51** 20–9
[28] Zhang L, Tonks M R, Gaston D, Peterson J W, Andrs D, Millett P C and Biner B S 2012 *J. Comput. Phys.* **236** 74–80
[29] Ackland G J and Thetford R 1987 *Phil. Mag.* A **56** 15–30
[30] Zhang Y, Millett P C and Tonks M 2011 *Comput. Mater. Sci.* **50** 3224–9
[31] Tonks M R, Zhang Y, Biner S, Millett P C and Bai X 2013 *Acta Mater.* **61** 1373–82